Journal of Electroanalytical Chemistry 922 (2022) 116707

Contents lists available at ScienceDirect

Journal of Electroanalytical Chemistry

journal homepage: www.elsevier.com/locate/jelechem

Role of carbon material surface functional groups on their interactions with aqueous solutions

A.A. Atchabarova [a], S.K. Abdimomyn [a,*], D.A. Abduakhytova [a], Y.R. Zhigalenok [a], R.R. Tokpayev [a], K.K. Kishibayev [a], T.N. Khavaza [a], A.P. Kurbatov [a], Y.V. Zlobina [a], T.J. Djenizian [b]

[a] Center of Physical Chemical Methods of Research and Analysis, Al-Farabi Kazakh National University, Almaty, Kazakhstan
[b] École Nationale Supérieure des Mines de Saint-Étienne, Saint-Etienne, France

ARTICLE INFO

Keywords:
Hydrothermal carbonization
Carbon material
Thermal carbonization
Walnut shell
Activated carbon
Functional groups

ABSTRACT

In this work, the fundamental study of the surface functional groups' role of the carbon material based on walnut shells in water solutions was studied. Functional groups (FG) were evaluated by Boehm's titration method, electrochemical impedance spectroscopy, spectrophotometric method, etc. The surface oxygen-containing functional groups (OCFG) was determined quantitatively by Boehm method: C(-C-OH) = 1.15 mmol/g; C(-C═O) = 0.87 mmol/g; C(–COOH) = 6.31 mmol/g. By the method of edge angle wetting the influence of OCFG on the formation of a hydrophilic functional layer on the surface of carbon material at different electrolyte media and adhesion works were found. The results of ζ-potential measurements as a function of solution pH allowed us to characterize the surface redox (acid-base) centers of the carbon material. Electrochemical impedance spectroscopy results show that surface OCFGs have a large influence on carbon material capacity characteristics.

1. Introduction

Carbon is a promising material in systems for water resources purification from heavy metals and organic pollutants and energy storage systems as electrode material.

A unique feature of carbon materials (CM) is the distribution of many different OCFG (–OH, -C═O, –COOH, -C─O─C- and their combinations). This condition allows concentrating on studying mechanisms and processes occurring at carbon/electrolyte phase boundary due to OCFG impact on electrochemical and adsorptive characteristics of carbon materials (specific capacitance increase, specific adsorption, pseudocapacitance redox reactions, etc.).

There are chemical and electrochemical modifications for forming surface functional layer; their advantage is condition variation simplicity: variation of solution pH, nature of electrolyte and modifier, potential and current sweep modes, etc. In work [1] authors study carbon fiber (CF) modified with HNO_3, O_3, and electrochemical modification for –COOH, -C═O formation and increase of adsorption capacity towards cadmium ions depending on pH. Surface functional groups (FG) dissociation with pH increasing leads to adsorption capacity increase towards Cd^{2+} through ion exchange mechanism. Authors of this work [2] studied electrochemical characteristics of microporous cokes activated by KOH and NaOH for use in supercapacitors, where a correlation between surface OCFG and electrode specific capacitance was observed. It was found that KOH activation at T < 700 °C leads to pseudofaraday contribution impedance resistance increase. Its leads to strong dependency on current density. In work [3] it was found significant anodic electrochemical modification influence on functional layer formation on carbon nanotubes surface for $[Ru(NH_3)_6]^{2+/3+}$, $[Fe(CN)_6]^{4-/3-}$ and $Fe^{2+/3+}$ redox reactions charge transfer increase.

Multiple methods can be applied for studying OCFG distribution and quantification [1]: Boehm titration [2], Fourier transform infrared spectroscopy (FTIR) [3], temperature-programmed desorption coupled with mass spectrometry (TPD-MS) [4], X-ray photoelectron spectroscopy (XPS) [5], and X-ray absorption near edge structure (XANES) spectroscopy [6]. The authors of work [10] systematically studied the influence of the nature of FG on the specific capacity of carbon electrodes (CE) by the temperature-program desorption (TPD) method. This allowed us to establish that in acidic aqueous electrolytes CO is mainly derived from hydroxyl, carbonyl, and quinone groups, while CO_2 is mainly derived from carboxyl, anhydride, and lactone groups.

Cyclic voltammetry and electrochemical impedance spectroscopy are applicable for fundamental research of carbon functional layer in aqueous environments. In this article [11] the wettability impact of

* Corresponding author.
E-mail address: abdimomyn03@gmail.com (S.K. Abdimomyn).

https://doi.org/10.1016/j.jelechem.2022.116707
Received 23 March 2022; Received in revised form 12 August 2022; Accepted 12 August 2022
Available online 23 August 2022

CE surface on capacitance increase was researched by the Electrochemical impedance spectroscopy method (EIS). It was shown that surface layer modification by extensive cycling increases speed of ions migration to the surface and mass transfer resistance, which facilitates CE specific capacitance increase [7]. Interesting observations are shown in [8] which researches concentration polarization impact on pseudocapacitive redox reactions of carbon material OCFG. Authors used cyclic voltammetry to find redox current peak at 0,55 V in acid water solutions; this is related only to H^+ concentration regardless of acid nature. After solution pH increase peak value lowering is not related to OH^- interaction with OCFG but related to H^+ absence in near-electrode space [9].

The presence of surface OCFGs and control of their amount using modification conditions allows forming carbon material surface functional layer of specific nature which can be further used for specific adsorption processes and supercapacitors.

The aim of this research is studying the behavior of the surface functional groups of carbon material in the pH range from −0.5 to 13 by cyclic voltammetry and the electrochemical impedance spectroscopy. Also, the characterization of acid-base adsorption centers by the method of adsorption indicator in the region of pK_a from 0.8 to 12.8 and measurement of ζ-potential in the working regions of pH.

2. Materials and methods

2.1. Reagents and equipment

The following reagents have been used in this research: K_2SO_4, Na_2SO_4, Na_2CO_3, $NaHCO_3$, NaOH; HCl; acetone, H_2SO_4, $K_4[Fe(CN)_6]$; $K_3[Fe(CN)_6]$ c.p. Sigma Aldrich; dehydrated ethanol, 99 %; ultrahigh-dispersity polyethylene powder (UDPEP) GUR®, USA; argon, c.p.

The following equipment were used for studying carbon materials: Planetary monomill FRITSCH PULVERISETTE 6; automatic potentiometric titrator ATP-02 with glass electrode; potentiostat–galvanostat BioLogic SP-300; potentiostat–galvanostat AutoLab 502 N.

2.2. Study object characteristics

Carbon materials (CM) based on walnut shells were obtained by hydrothermal carbonization (HTC) at T = 240 ^{0}C during 24 h stainless steel autoclave. The material to water ratio was 1: 2. To increase CM specific surface and form oxygen-containing functional groups, the material was activated with acute water steam (AAWS) at T = 800–850 ^{0}C during 60–70 min. Then sorbent was ground to 56 μm [10,11,42].

According to the results shown in Table 1, it was found that the activation of carbonizate of carbon material by acute water vapor leads to chemical conversion of the surface of carbon material. This leads to the destruction of the carbon matrix as well as the formation of oxygen functional groups. This is evidenced by the increase in the specific surface area by about 2 times. In addition, there is an increase in the average micropore size from 1.24 nm to 1.74 nm. The percentage of microporosity corresponds to the values of 87.5 and 84.09 %. A decrease in the average adsorption energy calculated by the Dubinin-Radushkevich equation is observed in the activation of carbon materials. However, the chemical sorption process prevails in these research objects since physical sorption processes have adsorption energy in the range of 1–8 kJ·mol^{-1} and chemisorption processes have adsorption energy > 8 kJ·mol^{-1} [12].

2.3. Preparation of mechanically strong carbon electrodes

A mechanically strong carbon electrode was made by mixing activated carbon and ultrahigh-dispersity polyethylene powder (UDPEP) GUR®, USA. The electrode has d cylindrical shape with a diameter of 0.8 cm and thickness of 0.2 mm. Electrode surface area was 1 cm^2. The carbon electrode mass was 10 mg.

Optimal conditions for obtaining mechanically strong carbon electrode were the following: P = 150 atm.; T = 130 ^{0}C; AC: binding ratio was 70: 30 %, respectively (w/w).

2.4. Determination of the surface functional groups amount by Boehm's titration method

1 g of activated carbon was allowed to stand in 0.1 M degassed basic solutions of various nature (Na_2CO_3, $NaHCO_3$, NaOH) for 24 h. Then, the excess of HCl was titrated with 0.1 M NaOH.

2.5. Determination of the carbon electrode water contact angle

To measure hydrophilic property by water contact angle on carbon electrode sitting drop method was used at various nature of electrolyte – 0.1 M Na_2SO_4 and K_2SO_4 [13] (Fig. 4). Contact angle change was observed using the SuperEyes B011 microscope and SuperEyes software.

2.6. Determination of ζ-potential at different electrolyte concentrations and pH values in solution

Determination of ζ-potential was performed by dynamic laser light scattering using Malvern Zetasizer NanoZS 90. 30 mg of activated carbon were put in 50 ml of background electrolyte (Na_2SO_4, K_2SO_4) solution with concentration variations from 0.1 mM to 1000 mM. Solution pH was adjusted using H_2SO_4 and NaOH, KOH, respectively. pH solution range was chosen to be within 0.5 and 12.0. Results of ζ-potential dependency on solution pH were statistically processed according to Student's *t*-test and Fisher's criterion. To study the linear correlation between two dependent variables of the same general totality and define correlation coefficient Pearson, Spearman, and Kendal correlations were used. To evaluate correlation coefficient constraint force Chaddock scale was used.

2.7. Electrochemical study on carbon electrodes

Electrochemical characteristics were studied using AutoLab 302 N galvanostat/potentiostat. Three-electrode electrochemical cell consisted of Ag/AgCl reference electrode (3.5 M KCl); electroactive carbon fabric was used as counter electrode; developed durable carbon electrode was used as the working electrode. The current collector was glass-carbon rods inserted into Teflon cylinders, which provided a clamping mode of attachment. Filter paper "green tape" acted as a membrane. Before each analysis, the glass-carbon rods were subjected

Table 1
Carbon materials specific area and porosity results comparison.

Activated carbon	S_{BET} [m^2·g^{-1}]	V_{total} [cm^3·g^{-1}]	V_{mN2} [cm^3·g^{-1}]	% of micropores	Micropore volume till 2 nm from N_2 [cm^3·g^{-1}]	Average pore width [nm]	Dubinin Radushkevich method Adsorption energy [kJ/mol]
HTC 240 °C/24 h	464.9	0.24	0.21	87.50	0.20	1.24	20.86
HTC 240 °C/ 24 h + AAWS 800 °C/ 1h	738.0	0.22	0.19	84.09	0.16	1.74	14.92

to successive polishing with abrasive paper of granularity P1000, P1500 and P2000, followed by polishing with diamond paste to a mirror shine. The volume of electrolyte varied from 2 to 4 ml.

2.8. Determination of the electroactive surface of carbon electrode

For further ion mass transfer to carbon electrode surface electroactive areas of electrode surface were defined in 0.005 M $K_4[Fe(CN)_6]$ and $K_3[Fe(CN)_6]$ solutions due to reversibility of this system. Due to linearity of I_p dependency on $v^{1/2}$, which indicates diffusion kinetics, surface electroactive areas (A) of studied carbon electrodes are calculated according to Randles–Sevcik equation:

$$I_p = 2,69 \cdot 10^5 \cdot n^{\frac{3}{2}} \cdot A \cdot D^{\frac{1}{2}} \cdot v^{\frac{1}{2}} \cdot C_0 \quad (1)$$

where I_p is peak current, A is electrode electroactive area, cm^2; D diffusion coefficient for $K_4[Fe(CN)_6]$ molecules in solution ($6.057 \cdot 10^{-6}$ cm^2/s [44]); v is speed of potential sweep, V/s; C is concentration of redox system in background electrolyte, mol/cm^3; n = 1 is number of electrons in redox process.

Roughness factors (electroactive to geometrical area ratio) were calculated for each indicating electrode according to f = A/S, where f is roughness factor; A is electroactive surface area; S is actual surface area (BET).

2.9. Influence of electrolyte pH on the electrochemical behavior of carbon electrode

To study solution pH influence on carbon electrode behavior 0,1 M Na_2SO_4 solution was chosen as background electrolyte. Solution pH adjustment was done with H_2SO_4 and NaOH. Cyclic voltammetry was used to study carbon electrode electrochemical and adsorption characteristics at 0.5–5 mV/s scan rates in the potential range between −1 V and 1 V.

2.10. Carbon electrodes electrochemical impedance spectroscopy

EIS was carried out for obtained carbon electrodes. Measurement potential corresponded to open circuit potential (OCP, OCV), frequency varied between 10 mHz and 1 MHz with 10 measuring points per decade. Cell (Fig. 2) was of pressure type, where the main working electrode was set onto glass-carbon base and pressed with polymethylmethacrylate mould, graphite rod was used as counter electrode, 0,5 M Na_2SO_4 with various pH values was used as electrolyte. Measurements were taken at 25 ^{0}C. Electrolyte pH was adjusted with H_2SO_4 and NaOH.

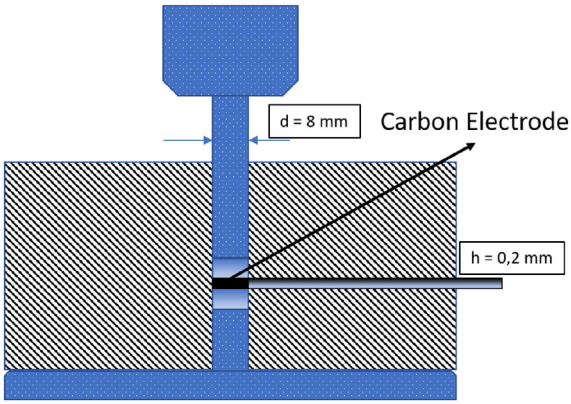

Fig. 1. Mould for carbon electrode making.

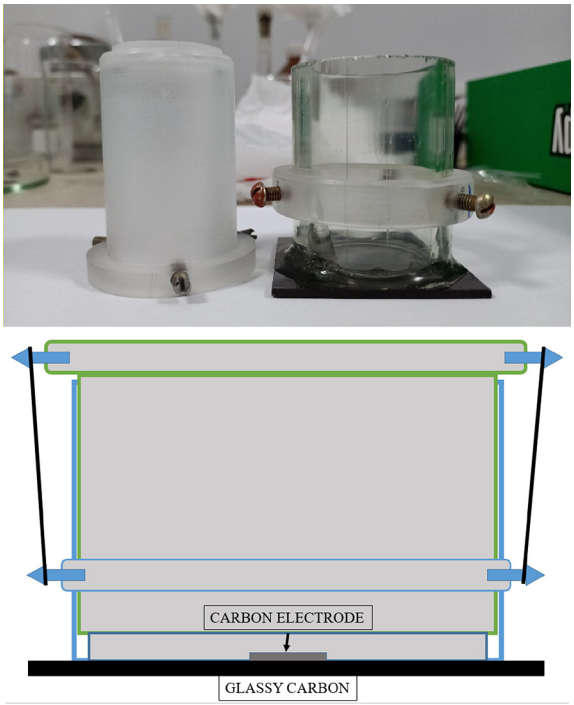

Fig. 2. Electrochemical cell for EIS.

2.11. Determination of carbon acidic-basic centers of material surface by adsorption indicator method

The selection of carbon material effective aliquot (a_{eff}) was carried out by taking series of kinetic curves pH = f (τ, a) while changing aliquot sample size. To obtain hydration kinetic curves, 10 ml distilled water was added into the potentiometric cell and after glass electrode potential stabilization aliquot samples of 0.01–0.2 g were added while taking the time. The first measurement of suspension pH was taken after 5–10 s, periods between the following measurements within the first minute were defined by hydration process kinetics. Then measurements were taken after 1.5, and 10 min depending on the curve, until pH values stabilization [10–21].

Regular 0.1 % solutions of used indicators were prepared according to GOST 4919.1–2016 [43].

Further, considering functional groups' quantitative determination by Boehm's method, indicator standard solutions were diluted 100-fold into 100.0 ml measuring flasks.

To perform spectrophotometric analysis of local acidity to determine the number of given acid strength adsorption centers (pKa), three standard solutions were prepared for chosen indicator Table 2 [22].

Solution #1 – «blind test» is measurement of A_0. The required amount of indicator standard solution was taken to 5–15 ml measurement tube with a measuring pipette and added distilled water until required amount is reached. This solution was used for indicator passing without a carbon sample.

Solution #2 is measurement of A_1. Carbon sample a_1 effective aliquot and the same amount of indicator as for solution 1 are added to dry measurement flask, brought to required amount with distilled water, and mix for 2 h in a mixer. In photometrical analysis of this solution indicator passing change due to its adsorption and pH change is taken into account.

Solution #3 is measurement of A_2 (correction). Carbon sample a_2 aliquot and 5–15 ml of distilled water are added to dry measurement flask and mixed for 2 h in a mixer. In this case, indicator adsorption process is eliminated but sample interaction with solvent influence on indicator passing – correction due to water environment pH change (increase or decrease) is taken into account.

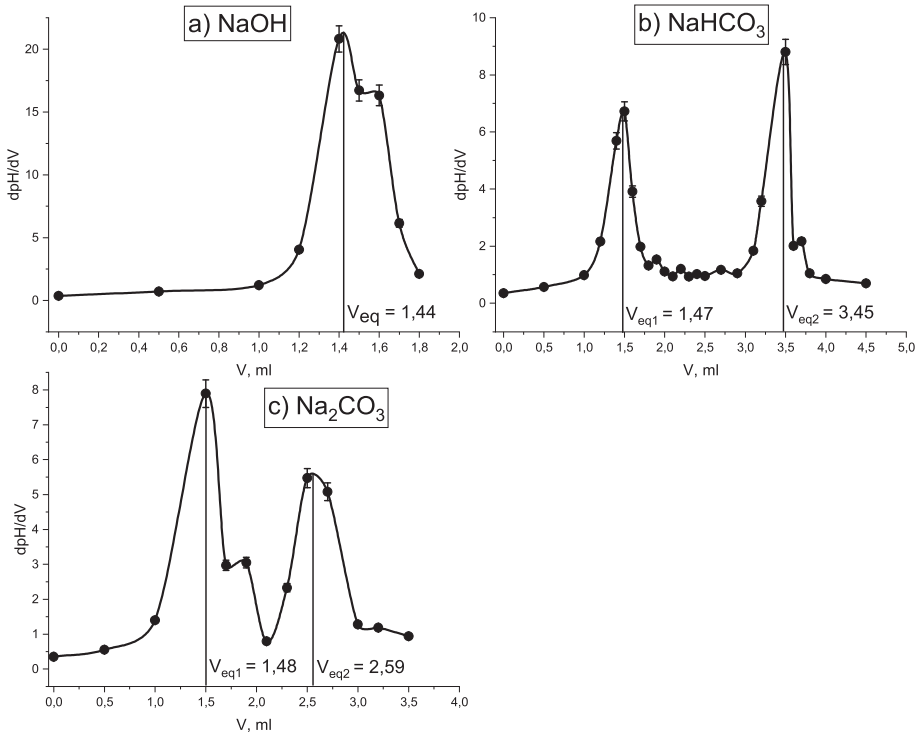

Fig. 3. Differential curves of reverse potentiometric titration after CM functional groups neutralization by 0.1 M basic solutions: NaOH (a), $NaHCO_3$ (b), Na_2CO_3 (c).

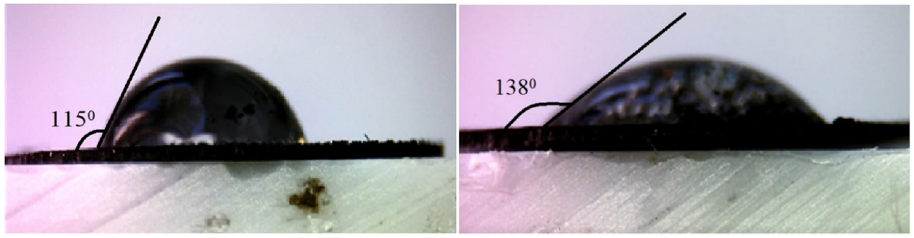

Fig. 4. Water contact angle at zero time: 0.1 M Na_2SO_4 (a) and K_2SO_4 (b).

Table 2
Acidic-basic and adsorption indicators.

#	Indicator	pKa	M_r, g/mol	Wavelength, λ, nm
1	Crystal violet	0.8	407.99	572
2	Methyl orange	3.5	327.33	464
3	Bromphenol blue	4.1	699.96	592
4	Methyl red	5.0	269.30	524
5	Alizarine red	5.5	360.27	428
6	Neutral red	7.6	288.78	530
7	Bromthymol blue	7.3	624.38	434
8	Thymol blue	8.8	466.59	436
9	Indigo carmine	12.8	422.38	610

After mixing solutions #2 and #3 were centrifuged for 1 h, then aliquot was taken for spectrophotometric analysis.

The number of centers $q_{c(pKa)}$ of given acid strength (pKa) was calculated according to the formula in equivalent to dry sorbent mass unit ($mol \cdot g^{-1}$).

$$q_{c(pKa)} = \frac{C_{ind}V_{ind}}{A_0}\left|\frac{|A_1 - A_0|}{a_1} \pm \frac{|A_2 - A_0|}{a_2}\right|, \quad (2)$$

where C_{ind} and V_{ind} are concentration (10^{-3} – 10^{-4} M) and aliquot part volume (1–3 ml) of indicator standard solution; signs (+) and (−) correspond respectively to multidirectional: $A_1 > A_0 < A_2$ ($A_1 < A_0 > A_2$) and unidirectional: $A_1, A_2 > A_0$ ($A_1, A_2 < A_0$) change of A_1 and A_2 in reference to A_0.

Then Hammet's acidity function was calculated (H_0). It is average surface acidity which is characterized through singular center acid strength value (pKa_c) as average value of all centers ($\sum q_{pKa}$):

$$H_0 = \overline{pKa_c} = \frac{\sum pKa_c \cdot q_{pKa}}{\sum q_{pKa}} \quad (3)$$

3. Results and discussion

3.1. Determination of the surface functional groups amount by Boehm's titration method

The reverse potentiometric titration method was used to determine quantities of carboxylic, hydroxylic, and carbonylic surface groups.

The results of reverse potentiometric titration according to Boehm's method are shown in Table 3. The calculation was carried out of the functional groups' concentration different nature distribution out per 1 g and 1 m^2 of CM surface based on the data.

Table 3
The concentration of functional groups on CM surface (hydrothermal carbonization 240 °C/24hr + AAWS 800 °C/1hr).

$C_i \cdot 10^3$, mol/g			$C_i \cdot 10^6$, mol/m^2		
C-OH	C═O	–COOH	C-OH	C═O	–COOH
1.15	0.87	6.31	1.53	1.15	8.37

It is assumed that the bases used neutralize all oxygen surface groups, depending on the strength of their acidity. Accordingly, $NaHCO_3$ primarily deprotonates –COOH and, Na_2CO_3 reacts with ether and lactone functional groups. In addition, NaOH neutralizes –OH as well as converts all surface oxygen-containing groups that enter into acid-base reactions in aqueous solutions [2].

The use of reverse potentiometric titration has a decisive advantage over direct titration. With degassing and the addition of 0.1 M HCl for further titration with 0.1 M NaOH, it is possible to increase the accuracy and reproducibility of the results. Before being left for a day, the argon-injected carbon samples were ultrasonically treated, it allows effective destruction of agglomerates and deprotonation of all surface groups [4].

3.2. Determination of the carbon electrode water contact angle

Because applying a drop of electrolyte onto a carbon electrode leads to non-equilibrium change of water contact angle, equilibrium state of the drop is set for zero time. Based on this, CE surface water contact angle was calculated for the zero time according to Young's equation [14]:

$$\gamma_{LV}cos\theta = \gamma^0_{SV} - \gamma_{SL} \quad (4)$$

If surface tension at CE-air borderline σs-g is higher than at CE-electrolyte borderline $\sigma_{s\text{-}l}$, then contact angle θ < 90 °C and the solid body surface is hydrophilic. Fig. 4 is shown that θ is equal to 65° for Na_2SO_4 and θ is equal to 42° for K_2SO_4. It is suggested that at CE surface is hydrophilic due to presence of functional groups (COOH, COH, OH, C—O—C, etc.) on the CE surface, working as hydrophilic centers. The angle decreases over time, which is evidence of surface chemical interaction (Fig. 5 a, c).

According to the adhesion work equation [14]:

$$W_{SLV} = \gamma_{LV}(1 + cos\theta) \quad (5)$$

W_{SLV} adhesion work was calculated at CE-electrolyte borderline (0.1 M Na_2SO_4 (A) and K_2SO_4 (B))-air. During approximation to the ordinate axis in W_{SLV} = f(t) dependence diagram adhesion work at zero time was found, which is W_{SLV} = 102 J/g for Na_2SO_4 and W_{SLV} = 127 J/g for K_2SO_4. According to reference data, commercially obtained AC with $S_{specific}$ = 1000–1900 m^2/g have adhesion work values within the range of 103–193 J/g [15].

In a comparison of electrolyte cation nature's influence on adhesion work and water contact angle, it was found that water contact angle and adhesion work values are higher for K^+ than for Na^+. This suggests surface OCFGs' higher affinity and Gibbs free energy to K^+ than

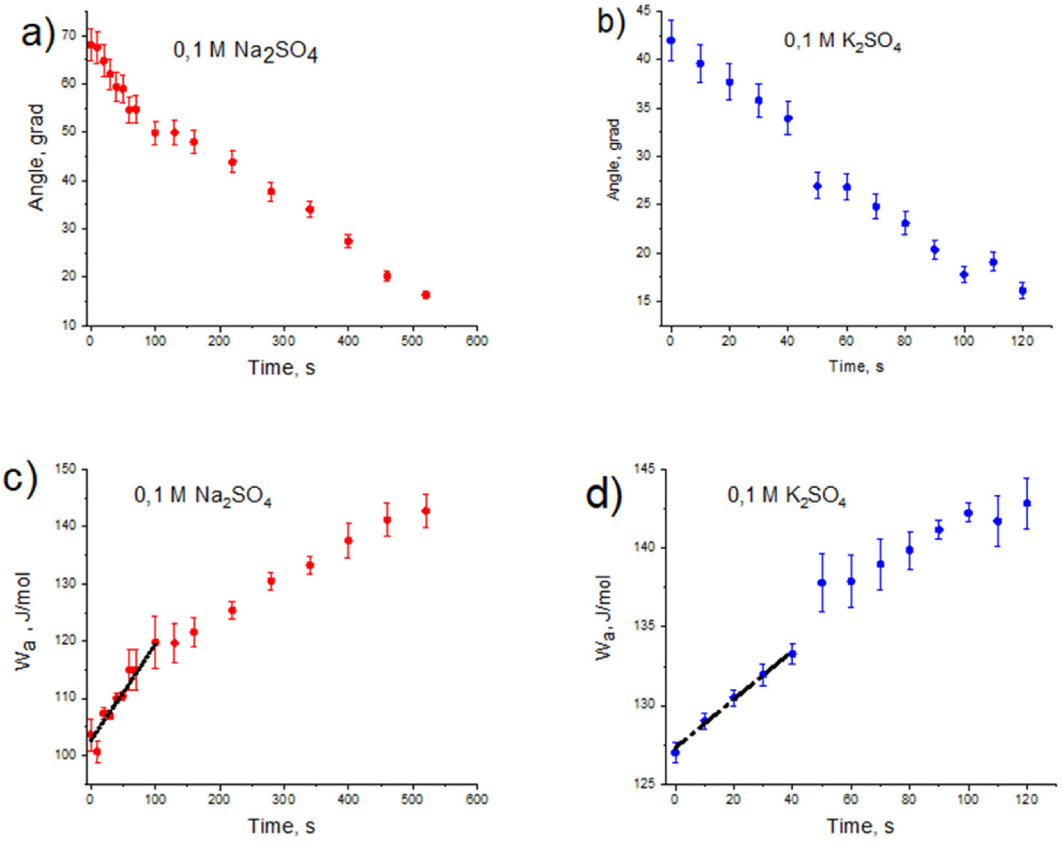

Fig. 5. Water contact angle (a,b) and adhesion energy over time (c,d).

Na^+, due to H_2O molecule stronger dipole moment with K^+, which leads to lower activity of water [16].

3.3. Determination of ζ-potential at different electrolyte concentrations and pH values

According to the Poisson-Boltzmann equation, ζ-potential distribution can be described using the linearized Poisson-Boltzmann equation. It is applicable to surface potentials within 5–80 mV with electrolyte concentration increase.

$$\frac{d^2\varphi}{dX^2} = \frac{c_0 e}{\varepsilon\varepsilon_0}\cdot\left(1+\frac{e\varphi}{k_B T}-1+\frac{e\varphi}{k_B T}\pm\cdots\right)\approx\frac{2c_0e^2}{\varepsilon\varepsilon_0 k_B T}\cdot\varphi \quad (6)$$

$$\varphi(x) = C_1\cdot e^{-kx} + C_2\cdot e^{kx} \quad (7)$$

C_1 and C_2 are constants determined by borderline conditions.

$$k = \sqrt{\frac{2c_0e^2}{\varepsilon\varepsilon_0 k_B T}} \quad (8)$$

Border-line conditions are determined as follows: when approaching surface, potential asymptotically goes towards surface potential, $\psi(x = 0) = \psi_0$, while at an infinitely big distance from the surface potential goes towards $\psi(x \to \infty) = 0$ expressions. From the first borderline condition results in $C_1 = \psi_0$ [26].

Therefore, the potential is determined as follows:

$$\varphi = \varphi_0 e^{-kx} \quad (9)$$

Potential is decreased according to exponential dependence. Quantitative characteristic is Debye length $\lambda_D = \kappa^{-1}$.

It is shown from Table 4 that electrolyte concentration leads to EDL diffusion layer contraction. This is reasonable because the more ions there are in the solution, the more effective surface charge screening [26].

It is shown from Fig. 6 that AC ζ-potential is described according to Poisson-Boltzmann particle distribution law. It is shown from the chart that slips potential correspond to negative value, which is characterized by the higher contribution of functional groups (–COH, –COOH, –OH, -C—O—C- etc.) on carbon material surface.

ζ-potential dependence on solution pH in various electrolyte nature is shown in Fig. 7. Research of solution pH influence on ζ-potential found out that pH which provides surface charge compensation is within 0–2 regardless of electrolyte nature, which is the evidence of AC acidic-basic features stemming from surface functional layer [27].

Test of hypothesis about dependencies generality for two selections of ζ-potential = f (pH) depending on electrolyte nature was performed according to Student's *t*-test and Fisher's criterion.

Table 4 is suggested that $t_{exp} < t_{0.05;\ 20\ table}$ and $F_{exp} < F_{0.05;\ 10;\ 10\ Table}$. It can be concluded that two samplings belong to the same general totality.

To determine linearity and correlation coefficient Pearson [17], Spearman, and Kendal [18] correlation was used. To evaluate correlation coefficient constraint force Chaddock scale [19] was used.

It was noticed that with AC ζ-potential value dismissal at pH = 12 linear correlation increased to a higher degree from 0.8 to 1 in Chaddock scale (Table 5), which encourages further research of AC ζ-potential change mechanisms in basic environments.

3.4. Determination of the electroactive area of carbon electrode

According to the results of carbon electrode surface electroactive area determination (Table 6), it was found that the maximum value is 7.785 cm^2 in 0.01 M Na_2SO_4.

Table 4
Statistical processing of AC ζ-potential change in electrolytes of different nature.

#	Electrolyte	Error dispersion, σ^2	Student's *t*-test		Fisher's criterion	
1	0.1 M Na_2SO_4	246.77	t_{exp}	0.507	F_{exp}	2.02
2	0.1 M K_2SO_4	498.15	$t_{0,05;\ 20\ table}$	2.086	$F_{0,05;\ 10;\ 10\ Table}$	3.07

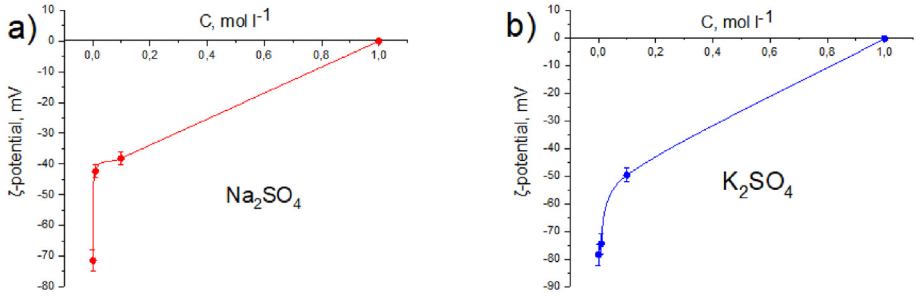

Fig. 6. AC ζ-potential distribution depending on electrolyte concentration.

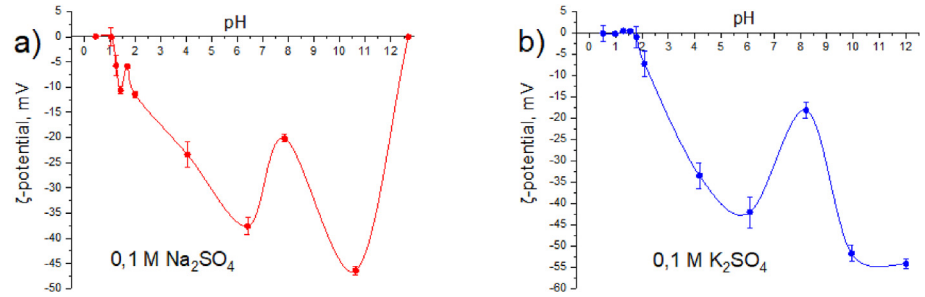

Fig. 7. AC ζ-potential change depending on pH in 0.1 M electrolyte solution 1: 2.

Table 5
Estimation of AC ζ-potential linear correlation in electrolytes of different nature.

Criteria	Correlation Pearson	Spearman	Kendal
With the point in pH = 12	0.62104	0.53636	0.52727
Without the point in pH = 12	0.96723	0.86667	0.77778

Table 6
Carbon electrode surface electroactive area at different ionic strength and cation nature.

#	Electrolyte	A, cm^2
1	0.01 M Na_2SO_4	7.785
2	0.01 M K_2SO_4	5.395
3	1 M Na_2SO_4	5.969
4	1 M K_2SO_4	5.985

Fig. 8b shows cyclic volt-ampere curves of carbon electrodes in $5{\cdot}10^{-3}$ M $K_3[Fe(CN)_6]$ + 0.01 M Na_2SO_4 electrolyte. As can be seen from the curves, there is an increase in current in both the anodic and cathodic potential windows in the region of negative potential windows. This is due to the capacitive accumulation of Na^+ in the pores of the carbon electrode. A further decrease in the current indicates the approach to the zero charge potential in the region of potentials 0.05–0.2 V [20]. The displacement of the $K_3[Fe(CN)_6]$ current peaks is associated with the influence of the external resistance of the electrochemical circuit, but, as observed on the cyclic curves, the displacement occurs linearly as the scan rate increases.

Due to this fact, this electrolyte was chosen for further research of CE behavior depending on solution pH. Besides, Na_2SO_4 has no specific adsorption towards electrode's carbon material, which is allowed to study faraday and pseudocapacitive redox reactions of CE.

3.5. Study of the carbon electrodes behavior depending on solution pH

According to volt-farad curves results (Fig. 9), at lower speed of potential sweep pseudocapacitive peaks are present, which is characterized by slow equilibrium appearance between H^+, Na^+, SO_4^{2-} ions and carbon within electrode matrix [21].

Besides, it was found that at pH < 2 and 0.45–0.55 V potentials there are strongly pronounced peaks in anode area, which is corresponded to quinone/hydroquinone system redox reactions [22]:

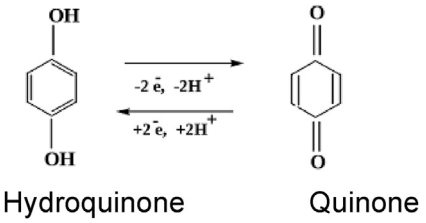

(10)

Hydroquinone Quinone.

The pseudocapacitive characteristics of graphite electrodes were studied in work [32]. They are electrochemically modified in 2.3 M H_2SO_4. The modification allowed increase amount of quinone, lactone, carboxylic and carbonylic functional groups on graphite electrode surface. It was contributed 70 % of electrode pseudocapacitance. Suggested schematic diagram of continuous reversible redox reactions between hydroxylic, carboxylic and carbonylic groups on CE corresponded to the following arrangement [32]:

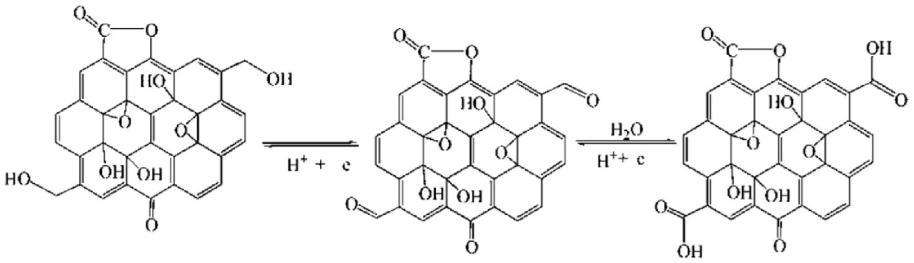

(11)

Redox reactions involving hydroxylic, carbonylic, carboxylic and lactone groups researched by authors of [23–26] studies can be categorized as pseudocapacitance. However, it is assumed that these reactions are only quasi reversible and gradual pseudocapacitance reduction is observed during long cycling process.

Volt-farad curves (Fig. 10) is shown the dependency of peak current (Ip) intensity increase at solution pH decrease within

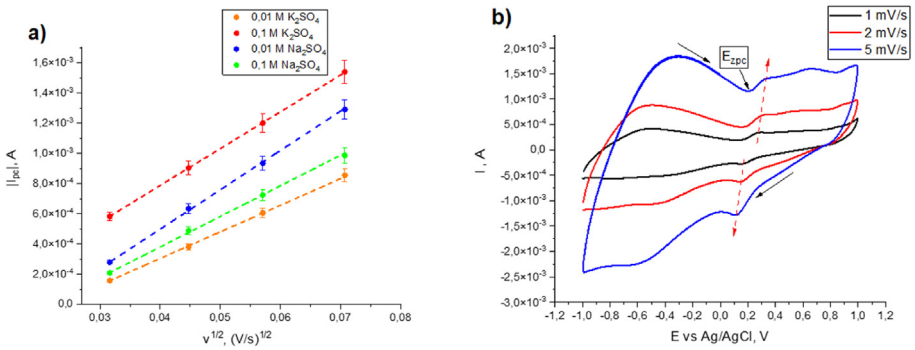

Fig. 8. I_p dependency on $v^{1/2}$ in $5{\cdot}10^{-3}$ M electrolyte $K_3[Fe(CN)_6]$ + (0.01–0.1 M) Na_2SO_4 / K_2SO_4 (a); Cyclic voltammetry curves of carbon electrodes in $5{\cdot}10^{-3}$ M $K_3[Fe(CN)_6]$ + 0.01 M Na_2SO_4 electrolyte (b).

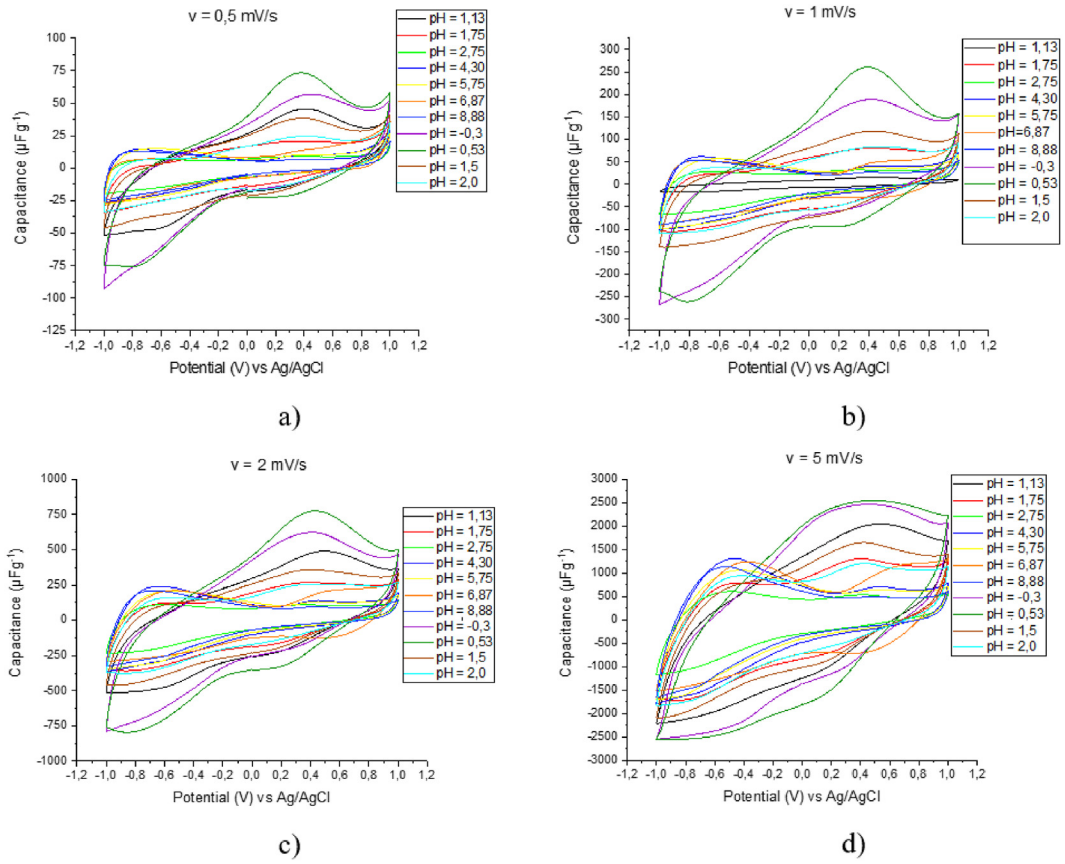

Fig. 9. Volt-farad curves at sweep speed 0.5 (a); 1 (b); 2 (c); 5 (d) mV/s CE in 0.1 M Na_2SO_4 solution depending on pH.

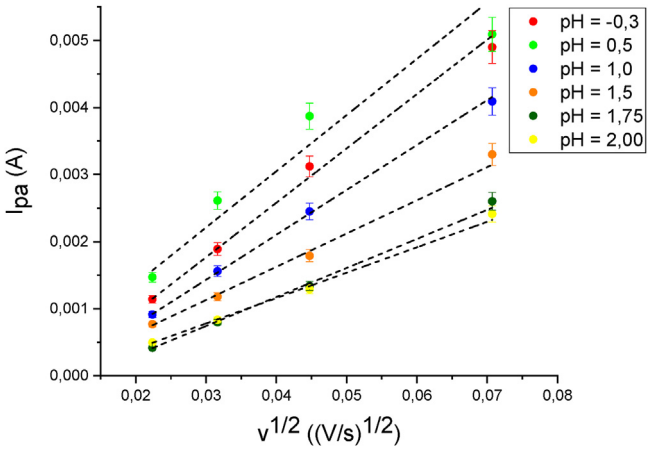

Fig. 10. Dependency of $I_{pa} = f(v^{1/2})$ at pH = -0.3; 0.5; 1.0; 1.5; 1.75; 2.0 in 0.1 M Na_2SO_4 solution.

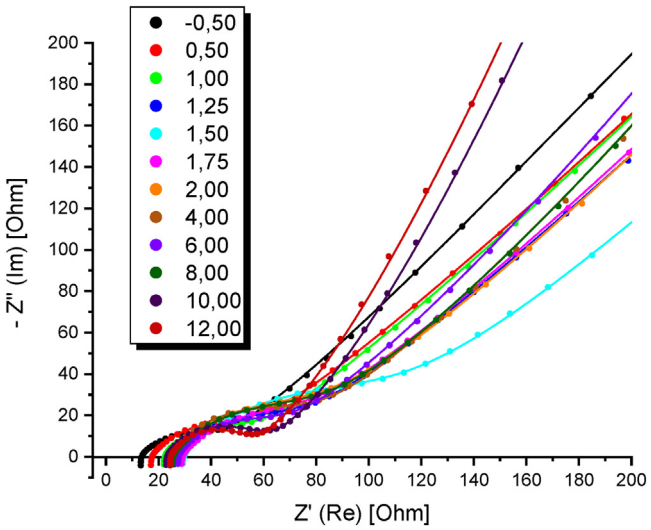

Fig. 11. Carbon electrode electrochemical impedance spectras depending on environment pH.

pH = 0.5–2.0 range. It is the evidence of hydrogen ions activity influence on redox reactions involving functional groups on CE surface according to the following scheme:

$$C\text{-}X^- + H^+ = C\text{-}X^-H^+, \quad (12)$$

where X = –OH, -C═O, –COOH, –NH. It (Fig. 11.) is assumed that at pH > 2Na^+ mobilities prevail over H^+, which leads to capacitative Na^+ ion accumulation in double electric layer (DEL). In case of pH < 2 concentration of H^+ significantly impacts Na^+ decrease in pores.

Peak offset potential (E_p) is observed with sweep speed increase, which suggests charge transfer resistance contribution in pores and ions transfer through EDL [27]. There is linear peak current (I_p) dependency on sweep square root ($v^{1/2}$) (Fig. 10), which suggests diffusion kinetics of redox process following Randles–Sevcik equation (1).

3.6. Carbon electrodes electrochemical impedance spectroscopy

Nyquist diagrams for carbon electrodes can be split into three areas as a consequence of processes happening due to alternate current stressing [28].

Change of Nyquist diagrams form is supposedly related to two factors. Let us focus on each of them.

Big variations of carbon electrode micropores and mesopores distribution are forming its high specific surface have special influence on diffusion to electrode surface, adsorption and intercalation of cations and anions into carbon material pores. Study [39] proves that carbon material pore shapes are the cause of condensation-capillary effect at carbon/electrolyte phase borderlines. Because of these pores influence solvent and ions penetration directly to carbon material surface, which leads to formation of carbon/electrolyte/air phase borderline.

According to these suggestions Nyquist diagrams are described in the following way:

1) while solution pH is within (-0.5) – 1.25, diagram describes involvement of spherical and octahedral pores, which indicates high proton mobility and filling of mainly micropores. Solution resistance R_s also rises from 12.55 to 25.13 at this pH range lower concentration of hydrogen ions, which proves the hypothesis about possibility of micropores filling with proton.
2) while solution pH is within 1.5 – 8.0, there is filling of cylindrical and triangular macropores (Fig. 10), which are characterized as hydrogen ions concentration reduction in electrolyte leading to EDL filling and formation mainly in mesopores of carbon material. If electrolyte pH rises from 1.5 to 2.0, R_s solution resistance reduces accordingly from 68.66 to 45.00 which indicates proton depletion as well as capillary condensation role increase in micropores. However, R_s solution resistance in neutral environment does not change rapidly and stays within 23.42–26.53. At pH = 8.0 solution resistance reduces to 44.93, which is related to OH^- ion mobility.
3) in alkaline environment pH = 10.0 – 12.0 there is reactivation and filling of carbon material micropores due to high OH^- ion mobility. At this pH range spherical and octahedral pores are filled (Fig. 10). R_s solution resistance is 22.57 и 24.28, respectively.

A more distinct difference in carbon electrode behavior in acid and alkaline environments is shown in Fig. 12.

Besides porosity and pore geometry, functional surface layer is another factor playing primary role in EDL formation and potential-determining ions adsorption at carbon/electrolyte borderline. Solution pH change has special influence on functional surface layer behavior in water systems.

Electrochemical impedance spectras (Fig. 10) were taken for carbon electrodes in solution of 0.5 M Na_2SO_4 depending on pH = -0.5; 0.5; 1.00; 1.25; 1.50; 1.75; 2.00; 4.00; 6.00; 8.00; 10.00; 12.00 to reveal redox surface centers influence mechanisms.

According to theoretical data on mechanisms occurring on carbon electrodes, there is following equivalent circuit describing these processes [29,30]:

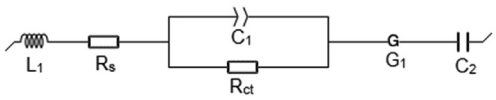

(13)

where, L_1 - inductance of current leads; R_s - resistance of electrolyte solution; C_1 - capacitance of double electric layer; R_{ct} - charge transfer resistance; G_1 - Gerrischer diffusion impedance; C_2 - capacitance due to oxygen-containing functional groups.

Real axis crossing at high frequencies and appearance of L inductivity is observed from results of carbon electrodes impedance spectra depending on solution pH. It forms effective series resistance (ESR). ESR is a consequence of resistance between outputs and electrodes as well as welding points. However, to eliminate this interference due to series of resistances inevitability identical counter-electrode, collector and outputs have to be used, which leads to working electrodes relevance [31]. As Table 7 shows, cell inductivity almost does

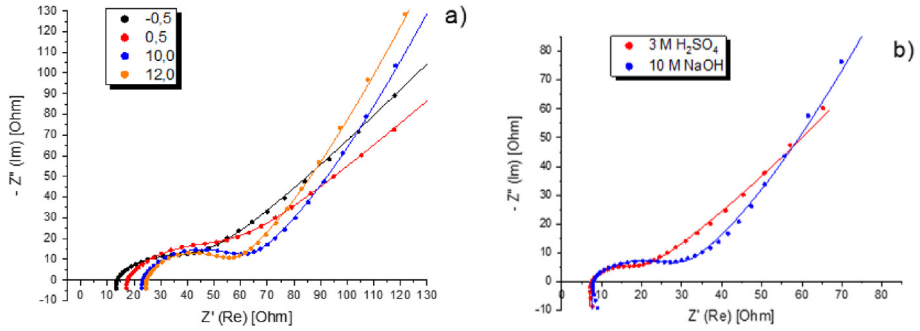

Fig.12. Carbon electrode electrochemical impedance spectras a) pH = -0.5; 0.5; 10.0; 12.0; b) 3 M H_2SO_4 and 10 M NaOH.

Table 7
Results of carbon material Nyquist curves equivalent circuits modeling depending on solution pH.

pH	L·10^7, h	R_s, Ohm	R_{ct}, Ohm	C_1·10^6, F	C_2·10^3, F	χ^2 * 10^{-3}
−0.77 (3 M H_2SO_4)	7.87	6.49	12.73	1.28	0.37	1.065
−0,50	7.94	12.55	27.92	1.60	1.69	1.824
0.50	7.49	16.63	32.4	1.69	2.14	1.146
1.00	7.65	21.03	29.75	0.79	1.33	0.509
1.25	7.49	25.13	40.51	1.06	1.39	0.225
1.50	7.59	27.97	68.66	1.09	1.30	0.613
1.75	7.19	27.97	37.63	1.36	0.77	0.225
2.00	7.39	24.21	45.00	1.33	0.70	0.288
4.00	7.40	23.42	43.72	0.78	0.41	0.959
6.00	7.30	26.53	33.82	0.73	0.34	0.539
8.00	7.47	24.39	44.93	1.30	0.40	0.271
10.00	7.25	22.57	35.29	0.93	0.50	2.437
12.00	7.25	24.28	28.03	1.23	0.52	5.586
13.00 (10 M NaOH)	7.61	7.45	20.07	3.91	3.33	4.156

not change at each measurement, which indicates elimination of interference.

EIS spectras are Nyquist diagrams typical for porous systems. At each solution pH value there is semi-circle crossing real axis in high-frequency area, forming R_{ct} charge transfer resistance at collector/carbon material and carbon/carbon borderlines. At medium frequency area there is 45° tilted line corresponding to ion diffusion towards electrode surface. However, at medium/low-frequency area with solution pH increase there is line rectification, which indicates capacitative prevalence at carbon/electrolyte borderline. Within solution pH = 1.00 – 12.00 R_s electrolyte resistance almost does not change. After $[H^+]$ concentration rise R_s reduces, which indicates high proton mobility as well high redox reaction ability with surface functional groups through adsorption of H_3O^+ [32]. In 10 M NaOH solution R_s falls to 7.447 Ohm, which indicates high proton mobility. However, comparison of R_s in 3 M H_2SO_4 and 10 M NaOH solutions shows that steric hindrance and ion hydration degree play significant role in ion interaction with surface layer.

The equivalent circuit used constant phase element (CPE) considering non-homogeneities modeling at carbon/electrolyte borderline and pores volume influence on ion diffusion non-homogeneity. CPE was transformed into double layer capacity according to the formula:

$$C_{dl} = Q^{\frac{1}{a}}\left(\frac{R_{Ohm}R_{CT}}{R_{Ohm}+R_{CT}}\right)^{(1-a)/a} \quad (14)$$

where C_{dl} is EDL capacity; Q is CPE; a is exponential factor indicating phase deflection, $0 \leq |n| \leq 1$; R_{Ohm} is ohmic resistance; R_{CT} is charge transfer resistance [33].

According to Nyquist curves equivalent circuits modeling results, there is correlation between EDL capacity OCFG pseudocapacity behavior (Fig. 13) [34]. Study [26] shows results of H_3O^+ adsorption with consecutive redox reactions on surface leading to formation of π-stretched surface electron cloud. Within pH = (−0.77) – 2.00 DEL capacity and pseudocapacity maximum is seen at pH = 0.5. This observation supports results of carbon materials cyclic voltammetry curves, where at pH = 0.5 pseudocapacity peak is observed at $E - E_{Ag/AgCl}$ = 0.5 – 0.55 V caused by quinone/hydroquinone system redox reactions [35].

In this study, the value of the Gerrischer diffusion impedance was not calculated, because the EDL capacity (C_1) and OCFG pseudocapacity (C_2) were important for us.

With pH solution increase at carbon material Nyquist curves and low-frequency area there is Warburg impedance shift towards capacity frequency-dependent pseudocapacity (line rectification) caused by surface adsorption-chemical transformations surface oxygen-containing functional groups via following mechanism [45]:

$$R\text{-}C_xO + [Na(H_2O)_n]^+ + e^- \; R\text{-}C_xONa(H_2O)_{n-y}. \quad (15)$$

In comparison to EIS results in acidic and basic solutions there is an obvious fact that alkaline metals have higher hydration degrees than H^+ [13]. However, due to OCFG presence and carbon surface hydrophilic property, Na + ions enter micropores because of hydration shell compression, forming EDL [46]. The authors of study [46] created a model where processes are divided into three segments; each of them is described DEL formation processes in micropores (<0,3 nm aperture).

Pearson criterion (χ^2) was used to check experimental Nyquist curves compliance with theoretical ones using equivalent circuits. It can be concluded from Table 7 that the results are reproducible and reliable.

3.7. Spectrophotometrical determination of carbon material surface acidic-basic center by adsorption indicator method

Carbon material surface charge kinetic changes in water environments are determined by two algorithmic processes; each of them can dominate. These processes are instant (10–10^{-5} s) relaxation of aprotonic centers and slow dissociation of protonic ones [36,37].

Aprotonic acids in water environment lead to concentration of H^+ suspension by adsorbing OH-groups as Bronsted acidic centers dissociation mechanism. If both groups are presented on the surface the solution pH is lowered. It's reflected total medium effect due to complexity of experimental differences during sorbent interaction with water. Similarly, aprotonic and protonic bases increase environment pH. The final outcome appears to be total effect of solvent interaction with carbon material surface which is reflected integral acidity change during hydration process. However, in a first approximation there is a possibility to evaluate surface center type due to suspension pH change character and speed [22].

It should be noted that pH-metrical research of solid-phase system should be preceded by choice of individual optimal sample aliquot mass (a_{eff}) at fixed volume of liquid phase [38,39]. Optimal aliquot size represents homogenized sample content, which allows reducing number of parallel determinations, increasing their reproducibility and reducing indeterminacy during statistical processing of outcomes.

Presented data analysis indicates that dependency pH_{eq} = f(a) follows the rule: with aliquot mass increase equilibrium state pH value in suspension system (pH_{eq}) rises, and after reaching certain acidity value it stops depending on sample mass, which is a consequence of suppressing the dissociation of its main type functional groups. The aliquot mass which provides pH stabilization at carbon/electrolyte borderline is = 0.05 g (Fig. 14a).

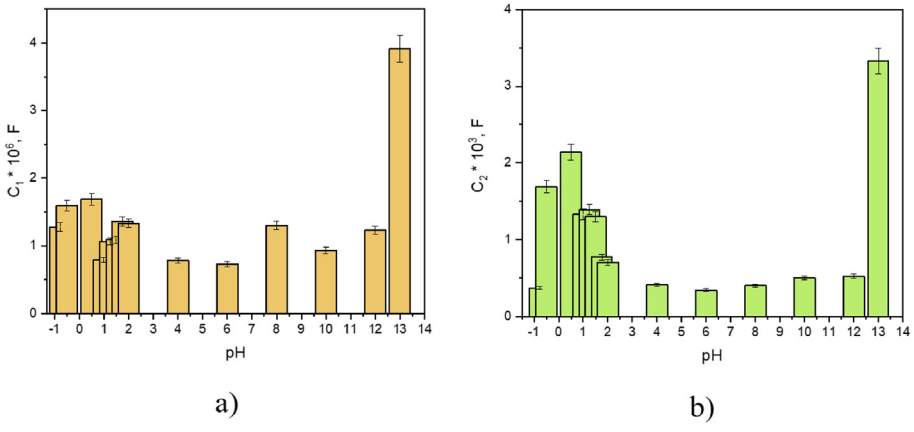

Fig. 13. EDL capacity (C_1) and OCFG pseudocapacity (C_2) dependence on solution pH.

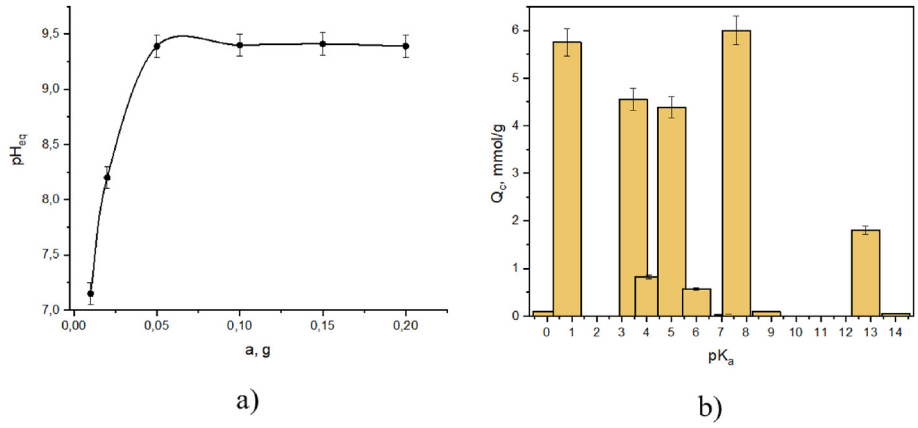

Fig. 14. a) pH dependence on aliquot mass for effective aliquot mass determination; b) Donor-acceptor adsorption centers distribution on carbon material surface.

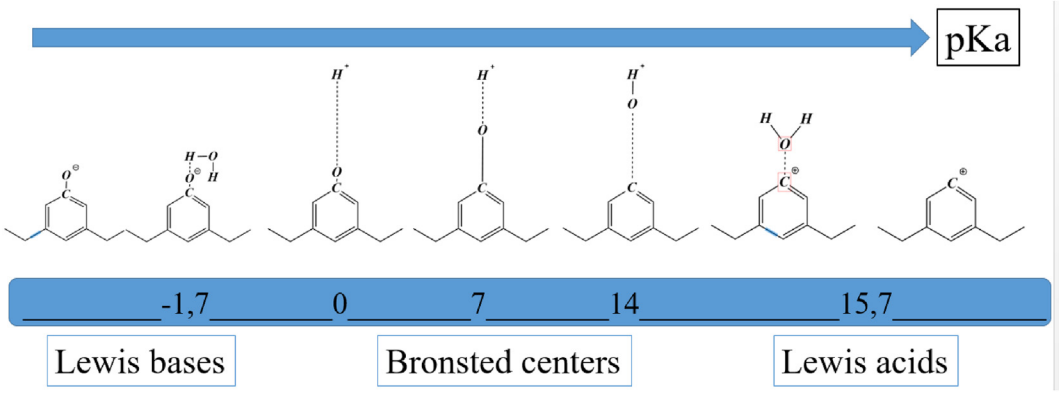

Fig. 15. Acidic-basic diagram of carbon material hydrated surface.

During carbon material surface (Fig. 15.) acidic-basic centers analysis it should be considered that indicators adsorption process follows Langmuir monomolecular adsorption mechanism, which suggests indicator monolayer on surface depending on solution pH, surface screening by "large" indicator molecule, surface non-homogeneities and roughness leading to single-point charge transfer due to Lewis and Bronsted acidic-basic centers are not taken into account.

Carbon material surface acidic-basic properties are characterized by the distribution of donor–acceptor centers, which were determined by acidic-basic indicators adsorption method.

As Fig. 14b shows, within pK_a = 0.0–3.5 distinctive adsorption centers can be seen. These acidic-basic centers are related to Bronsted protonic acids. Their acidity rises with increase of FG central oxygen atom accepting ability ($0 < pK_a < 7$). When charge (electron) is transferred from FG hydrogen atom to oxygen atom orbital, hydrogen abstraction occurs, which leads to formation of basic Lewis centers (C—O-, C-OO-), where in area $pK_1(H_2O)$ = -1.7–0.5 water molecules adsorption occurs by acidic type:

$$\equiv/C\text{-}\ \overset{OH}{\underset{/}{O}}\overset{=}{\cdots}H. \quad (16)$$

At pK_a = 5 there is peak corresponding to Q_c = 4.5 mmol/g, which is related to carboxylic and ethereal surface groups dissociation forming oxygen acceptor atoms in carboxyl-anion structure. Water molecule undergoes adsorption mechanism by acidic type through the following reaction [40,41]:

$$\equiv/COO\overset{OH}{\underset{/}{}}\overset{=}{\cdots}H. \quad (17)$$

Lewis bases are formed by oxygen atom two-electron orbitals and carbon matrix benzene ring and interact with charge transfer to water-acid energy level. Indicators-bases adsorption occurs in water solutions with $pK_a < 7$.

When carbon matrix donor properties strengthen and OH^- group is abstracted, Bronsted basic centers ($7 < pK_a < 14$) form Lewis acidic centers (C^{++}), where water molecules are adsorbed according to coordination mechanism [41]:

$$\equiv/C\overset{H}{\underset{/}{}}\overset{++}{\cdots}:OH. \quad (18)$$

Carbon matrix works as Lewis acid with vacant carbon level able to accept electron pair of water-base molecule. Indicators-acids adsorption occurs in water solutions with $pK_a > 7$.

As a result of dissociative hydroxylation, respective set of fixed protonic FGs – "integrated" acids and Bronsted bases of different strength, where water molecules physical (coulomb) adsorption is possible by acidic (19a) and coordination (19b) mechanisms, are produced on carbon material surface:

$$\equiv/C\overset{OH}{\underset{/}{}}\text{---}OH^{\delta-}\cdots H \qquad \equiv/C\text{--}O\overset{OH}{\underset{/}{}}{}^{\delta-}\cdots H \quad (19a)$$

$$\equiv/\ CO\ ---H^{\delta+}\cdots{:}OH \quad \equiv/COO---H^{\delta+}\cdots{:}OH \tag{19b}$$

Due to the presence of Lewis adsorption centers with lower water affinity within $pK_a < -1.7$ and $pK_a > 15.7$, these areas were not analyzed.

Thus, all mechanisms of dissociative and molecular water adsorption form functional hydroxylic-hydrate surface layer reflecting its acidic-basic properties.

Based on experimental data surface acidity function H_0 was determined. In this approximation, it is a "quasi-value" of surface energy evaluation. H_0 position on pH scale towards neutrality level determines correlation of acid and base centers of both protonic and aprotonic types, as well as their acidic strength. Hammet value H_0 for carbon material is equal to 4.93.

The adsorption indicator method allows point surface analysis of electrochemically and chemically modified carbon material to suggest adsorption process mechanisms for water resources purification from heavy metals and organic contaminants.

Further work on adsorption indicator method application will be focused on revealing solvent influence mechanism, specifically [21,22]:

1) Indicators adsorption without environment pH change:
   - indicators adsorption on Lewis and Bronsted centers of both types;
   - indicators adsorption on one-electron aprotonic centers with water molecules dissociating via homolytic mechanism;
2) Indicators adsorption on surface with environment pH change:
   - indicators adsorption on dissociating Bronsted centers;
   - indicators adsorption on Lewis centers including water molecules dissociating via heterolytic mechanism.

3.8. Distribution diagrams for carbon material surface OCFGs

Results of OCFG quantitative determination by Boehm titration, cyclic voltammetry and carbon material electrochemical impedance spectra allow making certain modeling assumptions considering nature of functional groups and influence of their relations to carbon matrix on behavior in water solutions. Results of Boehm titration show that –COOH, -C═O, –OH FGs are distributed on carbon material surface. According to this, carboxylic groups' dissociation is described by the following reaction:

$$1)\ RCOOH \leftrightarrow RCOO^- + H^+ \tag{20}$$

where R is carbon matrix. Dissociation constant can be described for this dissociation reaction:

$$K_{a,RCOOH} = \frac{[RCOO^-][H^+]}{[RCOOH]} \tag{21}$$

Equilibrium concentrations of dissociated forms can be expressed as follows:

$$[RCOOH] = \frac{[RCOO^-][H^+]}{K_{a,RCOOH}}[RCOO^-] = \frac{K_{a,RCOOH}[RCOOH]}{[H^+]} \tag{22}$$

$C_{RCOOH} = [RCOOH] + [RCOO^-]$, interval estimation of each form share can be calculated:

$$\alpha_{RCOOH} = \frac{[RCOOH]}{C_{RCOOH}} = \frac{[H^+]}{[H^+] + K_{a,RCOOH}} \tag{23}$$

$$\alpha_{RCOO^-} = \frac{[RCOO^-]}{C_{RCOOH}} = \frac{K_{a,RCOOH}}{K_{a,RCOOH} + [H^+]} \tag{24}$$

A similar calculation is done for hydroxylic group:

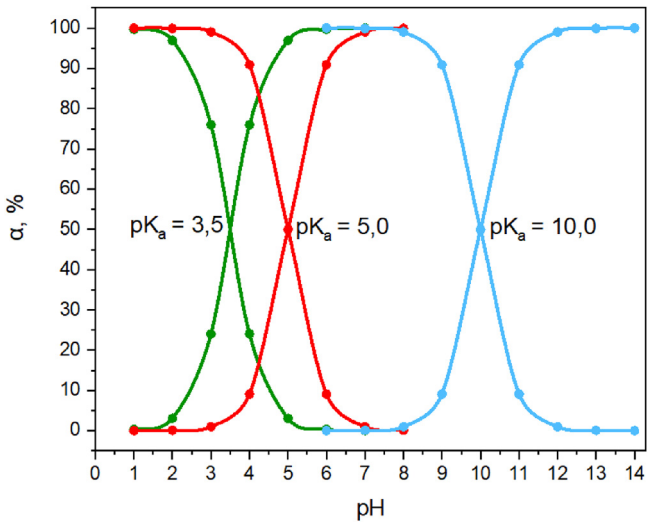

Fig. 16. Carbon material surface acidic-basic forms distribution diagram.

$$2)\ ROH \leftrightarrow RO^- + H^+ \tag{25}$$

$$K_{a,ROH} = \frac{[RO^-][H^+]}{[ROH]} \tag{26}$$

$$[ROH] = \frac{[RO^-][H^+]}{K_{a,ROH}}[RO^-] = \frac{K_{a,ROH}[ROH]}{[H^+]} \tag{27}$$

$C_{RCOOH} = [ROH] + [RO^-]$.

$$\alpha_{RCOOH} = \frac{[ROH]}{C_{ROH}} = \frac{[H^+]}{[H^+] + K_{a,ROH}} \tag{28}$$

$$\alpha_{RCOO^-} = \frac{[RO^-]}{C_{ROH}} = \frac{K_{a,ROH}}{K_{a,ROH} + [H^+]} \tag{29}$$

The distribution diagram of Hydroxylic and carboxylic surface FG dissociated forms is created according to the calculations above (Fig. 16).

4. Conclusion

This way, in this the research surface OCFGs was determined quantitatively by Boehm method: C(-C-OH) = 1.15 mmol/g; C(-C═O) = 0.87 mmol/g; C(–COOH) = 6.31 mmol/g. Contact angle method was used to reveal JCFG influence in hydrophilic functional layer formation on carbon material surface at different electrolyte nature. Also work of adhesion was found, which is WSLV = 106 J/g for Na_2SO_4 and WSLV = 127 J/g for K_2SO_4. Results of ζ-potential measurement depending on solution pH helped to characterize surface redox (acidic-basic) centers of carbon material. Based on volt-farad curves it was found that at pH = 0.5 and potentials 0.45–0.55 V there are distinctive peaks in the anodic area, which corresponds to pseudo redox reactions of quinone/hydroquinone system. EIS results show that surface OCFGs have a large influence on carbon material capacity characteristics. Some disadvantages were found, such as i) CM surface conductivity reduction; ii) prevention of ions entering pore channels as well as OCFG advantages at capacity increase; iii) increase of electrolyte wetting quality on CM surface; iv) pseudocapacitive redox reactions contribution; v) CM pores efficiency ratio increase due to quasi-reversible process of hydrated Na^+ charge/discharge. After solution pH increases mass transfer resistance decreases, which is caused by OCFG formation due to hydrated Na^+ implementation into micro-

pores. The adsorption indicator method was used to quantitatively determine redox (acidic-basic) centers, which helped to create surface OCFG distribution diagram. Hammet value H_0 for carbon material was determined, which is 4.93.

CRediT authorship contribution statement

A.A. Atchabarova: Project administration, Funding acquisition, Writing – review & editing. **S.K. Abdimomyn:** Conceptualization, Methodology, Formal analysis, Investigation, Writing – original draft. **D.A. Abduakhytova:** Conceptualization, Methodology, Investigation, Formal analysis, Writing – original draft. **Y.R. Zhigalenok:** Methodology, Investigation, Resources, Writing – original draft. **R.R. Tokpayev:** Formal analysis, Writing – review & editing. **K.K. Kishibayev:** Formal analysis, Writing – review & editing. **T.N. Khavaza:** Methodology, Investigation, Writing – original draft. **A.P. Kurbatov:** Conceptualization, Data curation, Supervision, Writing – review & editing. **Y.V. Zlobina:** Investigation, Formal analysis, Writing – original draft. **T.J. Djenizian:** Investigation, Formal analysis, Writing – review & editing.

Data availability

Data will be made available on request.

Declaration of Competing Interest

The authors declare that they have no known competing financial interests or personal relationships that could have appeared to influence the work reported in this paper.

Acknowledgement

This research was funded by the Science Committee of the Ministry of Education and Science of the Republic of Kazakhstan (Grant No. AP08957598 “The use of electrochemical methods for studying adsorption to characterize new carbon materials”).

References

[1] N. Li, J. Zhu, Q. Zha Quantitative and qualitative analyses of oxygen-containing surface functional groups on activated carbon, Chem. J. Chinese U. (2012) 13 10.3969/j.issn.0251-0790.2012.03.022.
[2] J. Schönherr, J. Buchheim, P. Scholz, P. Adelhelm Boehm Titration Revisited (Part I): Practical Aspects for Achieving a High Precision in Quantifying Oxygen-Containing Surface Groups on Carbon Materials, C. (2018) 4(2) 21 10.3390/c4020021.
[3] F. Meng, M. Song, Y. Wei, Y. Wang, The contribution of oxygen-containing functional groups to the gas-phase adsorption of volatile organic compounds with different polarities onto lignin-derived activated carbon fibers, ESPR. 26 (7) (2019) 7195–7204, https://doi.org/10.1007/s11356-019-04190-6.
[4] J. Schönherr, J.R. Buchheim, P. Scholz, P. Adelhelm Boehm Titration Revisited (Part II): A Comparison of Boehm Titration with Other Analytical Techniques on the Quantification of Oxygen-Containing Surface Groups for a Variety of Carbon Materials, C. 4(2) (2018) 22. 10.3390/c4020022.
[5] L. Li, X. Yao, H. Li, Z. Liu, W. Ma, X. Liang, Thermal Stability of Oxygen-Containing Functional Groups on Activated Carbon Surfaces in a Thermal Oxidative Environment, J. Chem. Eng. Japan/JCEJ 47 (1) (2014) 21–27.
[6] K. Kim, P. Zhu, N.a. Li, X. Ma, Y. Chen, Characterization of oxygen containing functional groups on carbon materials with oxygen K-edge X-ray absorption near edge structure spectroscopy, Carbon 49 (5) (2011) 1745–1751.
[7] Y. He Separating Current from Potential Sweep Method of Electrochemical Kinetics for Supercapacitors, arXiv.5 (2017) 1–10. 10.48550/arXiv.1702.08116.
[8] H.A. Andreas, B.E. Conway Examination of the double-layer capacitance of an high specific-area C-cloth electrode as titrated from acidic to alkaline pHs, Electrochim. Acta. 51(28) (2006) P. 6510–6520 10.1016/j.electacta.2006.04.045.
[9] H.P. Boehm, Some aspects of the surface chemistry of carbon blacks and other carbons, Carbon 32 (5) (1994) 759–769.
[10] A.A. Atchabarova, R.R. Tokpayev, A.T. Kabulov, S.V. Nechipurenko, R.A. Nurmanova, S.A. Yefremov, M.K. Nauryzbayev New electrodes prepared from mineral and plant raw materials of Kazakhstan, Eurasian Chem.-Technol. J. 18(2) (2016) 141–147. 10.18321/ectj440.
[11] A. Atchabarova, R. Tokpayev, A. Kabulov, S. Nechipurenko, S. Yefremov, M. Nauryzbayev Elaboration of electrodes for electrochemical processes based on new carbon-containing materials, Bull. Univers. Karaganda-Chemistry, 2016. - Vol. 83. - P. 66–71.
[12] A.L. Cazetta, A.M.M. Vargas, E.M. Nogami, M.H. Kunita, M.R. Guilherme, A.C. Martins, T.L. Silva, J.C.G. Moraes, V.C. Almeida, NaOH-activated carbon of high surface area produced from coconut shell: Kinetics and equilibrium studies from the methylene blue adsorption, Chemical Engineering J. 174 (1) (2011) 117–125, https://doi.org/10.1016/j.cej.2011.08.058.
[13] B. Jia, L. Zou, Wettability and its influence on graphene nansoheets as electrode material for capacitive deionization, Chem. Phys. Lett. 548 (2012) 23–28, https://doi.org/10.1016/j.cplett.2012.06.016.
[14] A.W. Adamson Physical Chemistry of Surfaces, A Wiley-Interscience publication. (1982) pp. 664.
[15] D.S. Dmitriev, M.V. Ivakhiv, D.V. Agafonov, Investigation of Lyophility of Activated Carbons Used in Technology of Supercapacitors, Bull. St PbSIT (TU) 44 (70) (2018) 21–25.
[16] M. Yu, Volfkovich Capacitive water deionization (review), Electrochemistry 56 (1) (2020) 20–55.
[17] B.Y. Lemeshko, A.W. Tanaseychuk Investigations of Estimated Correlation Coefficient Distribution Depending on Real Correlation Level (2007) 288 10.1109/APEIE.2006.4292562.
[18] M.D. Kendall, A. Styuart, Statistical inferences and connections, M, Nauka (1973) 899.
[19] G.T. Frumin, N.l. Bolotova, Prediction of Metal Ion Toxicity Using Ion Characteristics, Russ. J. Gen. Chem. 89 (13) (2019) 2746–2750.
[20] A.N. Frumkin, O.A. Petrii, B.B. Damaskin Potentials of Zero Charge, Comprehensive Treatise of Electrochemistry (1980) 221–289.
[21] A.N. Frumkin Potentials of zero charge, M., Nauka (1979) pp. 259.
[22] X. Fan, Y. Lu, H. Xu, X. Kong, J. Wang, Reversible redox reaction on the oxygen-containing functional groups of an electrochemically modified graphite electrode for the pseudo-capacitance, J. Mater. Chem. 21 (46) (2011) 18753.
[23] M.G. Sullivan, B. Schnyder, M. Bärtsch, D. Alliata, C. Barbero, R. Imhof, R. Kötz, Electrochemically Modified Glassy Carbon for Capacitor Electrodes Characterization of Thick Anodic Layers by Cyclic Voltammetry, Differential Electrochemical Mass Spectrometry, Spectroscopic Ellipsometry, X-Ray Photoelectron Spectroscopy, FTIR, and AFM, J. Electrochem. Soc. 147 (7) (2000) 2636, https://doi.org/10.1149/1.1393582.
[24] M. Mastragostino, F. Soavi, C. Arbizzani Electrochemical Supercapacitors, Advances in Lithium-Ion Batteries. (2002) 481–505.
[25] C.A. Richard, N.B. Philip, L. Jacek Electrochemistry of Carbon Electrodes, Wiley (2015), pp. 474.
[26] E. Frackowiak, B. Francois, Carbon materials for the electrochemical storage of energy in capacitors, Carbon. 39 (2001) 937–950, https://doi.org/10.1016/S0008-6223(00)00183-4.
[27] S. Kokhmetova, T. Kan, F. Malchik, A. Galeyeva, T. Djenizian, A. Kurbatov, Effect of the MoS_2 surface layer on the kinetics of intercalation processes in the NaFe$(SO_4)_2$/C composite, Mater. Today Commun. 28 (2021), https://doi.org/10.1016/j.mtcomm.2021.102723 102723.
[28] Y. He, Y. Zhang, X. Li, Z. Lv, X. Wang, Z. Liu, X. Huang, Capacitive mechanism of oxygen functional groups on carbon surface in supercapacitors, Electrochimica Acta 282 (2018) 618–625.
[29] H. Keiser, K.D. Beccu, M.A. Gutjahr, Abschätzung der porenstruktur poröser elektroden aus impedanzmessungen, Electrochimica Acta 21 (8) (1976) 539–543.
[30] X. Liu, Y. Wang, L. Zhan, W. Qiao, X. Liang, L. Ling Effect of oxygen-containing functional groups on the impedance behavior of activated carbon-based electric double-layer capacitors, J. Solid State Electrochem. 15(2) (2011) 413–419 10.1007/s10008-010-1100-2.
[31] R. Kötz, M. Carlen, Principles and applications of electrochemical capacitors, Electrochim. Acta. 45 (2000) 2483–2498, https://doi.org/10.1016/S0013-4686(00)00354-6.
[32] C.T. Hsieh, H. Teng, Influence of oxygen treatment on electric double-layer capacitance of activated carbon fabrics, Carbon. (40)5 (2002) 667–674, https://doi.org/10.1016/S0008-6223(01)00182-8.
[33] J. Friedl, U. Stimming, Determining Electron Transfer Kinetics at Porous Electrodes, Electrochimica Acta. 227 (2017) 235–245, https://doi.org/10.1016/j.electacta.2017.01.010.
[34] G. Arabale, D. Wagh, M. Kulkarni, I.S. Mulla, S.P. Vernekar, K. Vijayamohanan, A. M. Rao, Enhanced supercapacitance of multiwalled carbon nanotubes functionalized with ruthenium oxide, Chem. Phys. Lett. 376 (1-2) (2003) 207–213.
[35] C. Singh, A. Paul, Physisorbed Hydroquinone on Activated Charcoal as a Supercapacitor: An Application of Proton-Coupled Electron Transfer, J. Phys. Chem. C 119 (21) (2015) 11382–11390.
[36] V.F. Kiselev, O.V. Krylov Electronic phenomena in adsorption and catalysis on semiconductors, M., Nauka (1979) pp. 233.
[37] Ch. Kittel Introduction to solid state physics, M., Nauka (1978) pp. 791.
[38] A.P. Nechiporenko, A.I. Kudryashova Surface acidity function of solid oxides, Izvestiya SPbGUNiPT (32007) 14–24.
[39] A.P. Nechiporenko Donor-acceptor properties of the surface of solid oxides and chalcogenides, Thesis (1995) pp. 488.
[40] A.P. Nechiporenko, Donor-acceptor properties of the surface of solid-phase systems. The indicator method, Tutorial. SPb.Lan (2017) 284 p.
[41] K.V. Ikonnikova, Theory and practice of pH-metric determination of the solids surface acid-base properties, Tomsk, TPU (2011) 85 p.
[42] K.K. Kishibayev, J. Serafin, R.R. Tokpayev, T.N. Khavaza, A.A. Atchabarova, D.A. Abduakhytova, Z.T. Ibraimov, J. Sre´nscek-Nazzal Physical and chemical properties of activated carbon synthesized from plant wastes and shungite for

CO_2 capture, J. Environ. Chem. Eng. 9 (2021) 106798 10.1016/j.jece.2021.106798.
[43] GOST 4919.1-2016 – Reagents and highly purified materials. Indicator solution preparation methods.
[44] A.A. Nikiforova Electrochemical sensors based on carbon nanomaterials for the quantitative determination of a potential drug substance, Thesis (2021) pp. 75